Click Here for Full Article

Hydrothermal circulation within the Endeavour Segment, Juan de Fuca Ridge

H. Paul Johnson

School of Oceanography, University of Washington, Seattle, Washington 98195-7940, USA
(johnson@ocean.washington.edu)

Maurice A. Tivey

Department of Geology and Geophysics, Woods Hole Oceanographic Institution, Woods Hole, Massachusetts 02543, USA

Tor A. Bjorklund and Marie S. Salmi

School of Oceanography, University of Washington, Seattle, Washington 98195-7940, USA

[1] Areas of the seafloor at mid-ocean ridges where hydrothermal vents discharge are easily recognized by the dramatic biological, physical, and chemical processes that characterize such sites. Locations where seawater flows into the seafloor to recharge hydrothermal cells within the crustal reservoir are by contrast almost invisible but can be indirectly identified by a systematic grid of conductive heat flow measurements. An array of conductive heat flow stations in the Endeavour axial valley of the Juan de Fuca Ridge has identified recharge zones that appear to represent a nested system of fluid circulation paths. At the scale of an axial rift valley, conductive heat flow data indicate a general cross-valley fluid flow, where seawater enters the shallow subsurface crustal reservoir at the eastern wall of the Endeavour axial valley and undergoes a kilometer of horizontal transit beneath the valley floor, finally exiting as warm hydrothermal fluid discharge on the western valley bounding wall. Recharge zones also have been identified as located within an annular ring of very cold seafloor around the large Main Endeavour Hydrothermal Field, with seawater inflow occurring within faults that surround the fluid discharge sites. These conductive heat flow data are consistent with previous models where high-temperature fluid circulation cells beneath large hydrothermal vent fields may be composed of narrow vertical cylinders. Subsurface fluid circulation on the Endeavour Segment occurs at various crustal depths in three distinct modes: (1) general east to west flow across the entire valley floor, (2) in narrow cylinders that penetrate deeply to high-temperature heat sources, and (3) supplying low-temperature diffuse vents where seawater is entrained into the shallow uppermost crust by the adjacent high-temperature cylindrical systems. The systematic array of conductive heat flow measurements over the axial valley floor averaged ~150 mW/m^2, suggesting that only about 3% of the total energy flux of ocean crustal formation is removed by conductive heat transfer, with the remainder being dissipated to overlying seawater by fluid advection.

1. Introduction

[2] The location of seawater recharge zones relative to the focused high-temperature fluid discharge sites defines the geometry of subsurface hydrothermal fluid circulation cells. This geometry provides insight into the path lengths of circulation, which are required to estimate reservoir volumes, fluid velocities and residence times of subseafloor fluid flow. Three models for the geometry of circulation cell pathways have been suggested: (1) across-axis circulation with fluid flowing from either the outer ridge flanks into the central axial valley, or from one axial valley bounding fault to the opposite bounding fault [e.g., *Williams et al.*, 1979; *Johnson et al.*, 1993; *Villinger et al.*, 2002]; (2) circulation cells parallel to the spreading axis and associated with linear fault zones oriented along-strike of the axis [e.g., *Lowell et al.*, 1995, 2007; *Rabinowicz et al.*, 1999; *Wilcock*, 1998; *Tolstoy et al.*, 2008]; or (3) circulation organized into thin annular-shaped cylinders of seawater recharge surrounding active discharge regions [e.g., *Coumou et al.*, 2008].

[3] It has been difficult to discriminate between these various models because of a lack of data on the geometry of subsurface fluid flow at the spreading axis. While sites of active discharge are relatively easily defined, it has been difficult to identify sites of active recharge. Detailed measurements of conductive heat flow around vent sites and in the adjacent rift valley and flanking ridges is one type of measurement that could shed light on this issue. However, until very recently this measurement has been impossible to make on young unsedimented ocean crust. Here we report a novel application of a Thermal Blanket device to collect detailed conductive heat flow measurements on young ocean crust in an area that hosts ongoing hydrothermal activity, to determine if such measurements can provide a first-order assessment of fluid circulation geometry. The Main Endeavour Field (MEF) of the Juan de Fuca Ridge provides a well-studied example of a large, active hydrothermal system at a mid-ocean ridge (Figure 1), and from 2001 to 2003 it was the site of a systematic array of seafloor conductive heat flow measurements using Thermal Blanket technology [*Johnson and Hutnak*, 1998; *Johnson et al.*, 2006].

2. Heat Flow Measurements Using Thermal Blankets

[4] We have developed a new instrument to make conductive heat flow measurements on unsedimented seafloor consisting of a thin sheet of water-saturated open cell foam with thermistors mounted on both sides [*Johnson and Hutnak*, 1997, 1998; *Johnson et al.*, 2006]. When placed on the seafloor, the conductive thermal gradient from the underlying rock is transferred to the blanket while the internal foam matrix suppresses any internal convection of seawater within the blanket. The thermal conductivity of the foam material and blanket covering is negligible (<1%) compared to the mass of the blanket foam pore water. Laboratory tests demonstrate that the thermal conductivity of the saturated foam is identical, within measurement error, to that of non-convecting seawater [*Johnson and Hutnak*, 1998]. In addition to the internal open cell foam, the other components of the blanket are the fabric outer sheath, a heavy liquid-filled ($CaCl_2$-saturated) and lead-weighted outer rim to provide a tight thermal seal with the seafloor, plus floats and handles for deployment by remotely operated vehicle (ROV; Figure 2). The area of the circular blanket is ~1 m², and self-contained Antares thermistor/data loggers are used with a temperature resolution rated at ±0.001°C. Normal operations include 1 thermistor on the upper surface of the blanket and two thermistors on the lower surface, although many deployments used only one thermistor on each side (Figure 2). An example of the data is shown in Figure 3.

3. Endeavour Segment of the Juan de Fuca Ridge

[5] Hydrothermal discharge zones in the Endeavour Segment have been well studied (http://www.ridge2000.org/science/iss/references.php?site=Endeavour) and lists of recent references are available from *Van Ark et al.* [2007] and *Larson et al.* [2009]. The thermal blanket experiments described here were conducted over 3 cruises, using RV *Thompson* and ROV *Jason II*, in 2001 as part of the original NSF RIDGE program, and in 2002, and 2003 as part of the Life in Extreme Environments (LExEN) Program. A total of 46 deployment sites were attempted and these were concentrated around
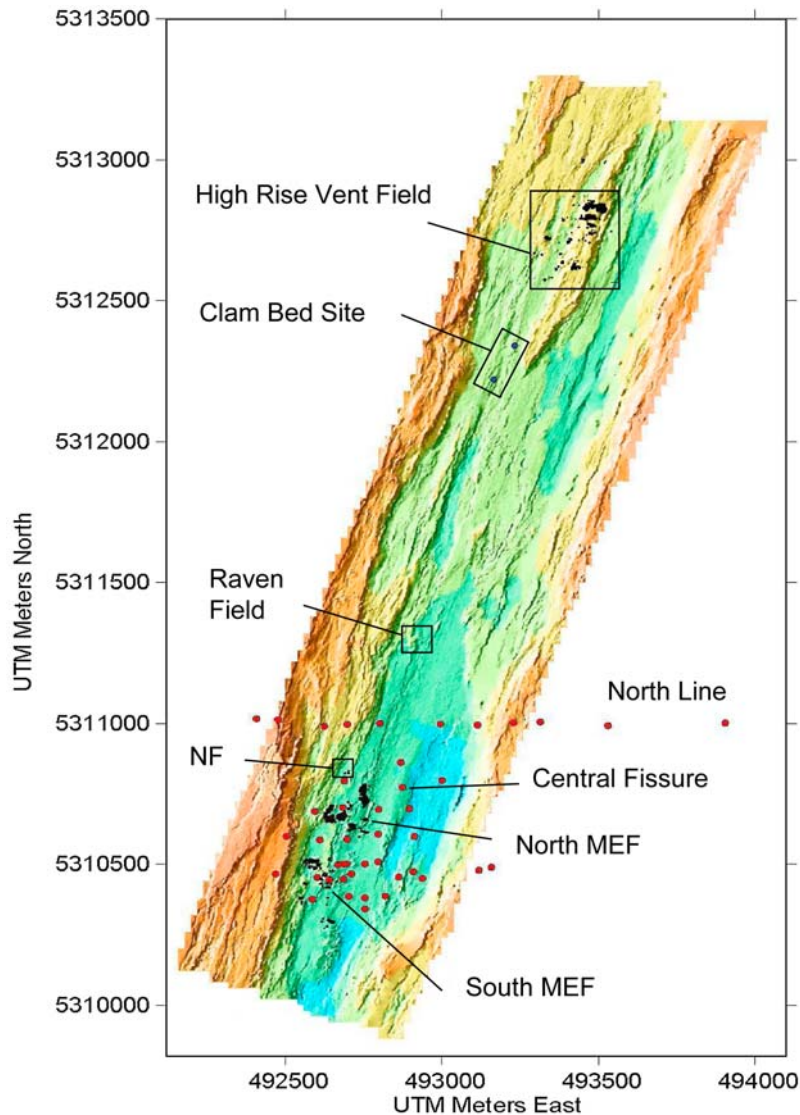
Figure 1. Endeavour Segment of the Juan de Fuca Ridge between Main Endeavour and High Rise Vent Fields, near 47°N and 129°W. Bathymetry data are from SM2000 scanning sonar survey. Red dots are thermal blanket deployment sites. North and South Main Endeavour Fields (N-MEF and S-MEF), New Field (NF), Raven Field, and High Rise Field are high-temperature vent fields with sulfide deposits shown in black. The central valley fissure described in section 6 is also labeled. Coordinates shown are UTM meters.

the North and South Main Endeavour vent Fields (N-MEF, S-MEF), including the "New Field" (NF) located ~100 m north of N-MEF (Figure 1). Forty-three of the 46 thermal blanket stations produced useful conductive heat flow data (Table 1). The blanket deployments were conducted in concert with a systematic ROV geophysical survey of the axial valley that encompassed both the MEF, NF and High Rise hydrothermal vent fields (Figure 1).

[6] In addition to a cluster of 32 stations around the active N-MEF and S-MEF vent fields, an additional linear array of 11 thermal blanket stations was deployed across the axial valley, oriented perpen-

dicular to the spreading axis and located 300 m north of the N-MEF vent area (North Line; Figure 1). This cross-axis array was designed to characterize the conductive heat flux of a section of the axial valley between the MEF and High Rise (2 km to the north; see Figure 1) vent fields that was unaffected by active hydrothermal fluid discharge. This initial goal was not realized as the easternmost thermal blanket stations showed low heat flow associated with active recharge and the western edge of the valley revealed a previously undetected area of warm fluid discharge.
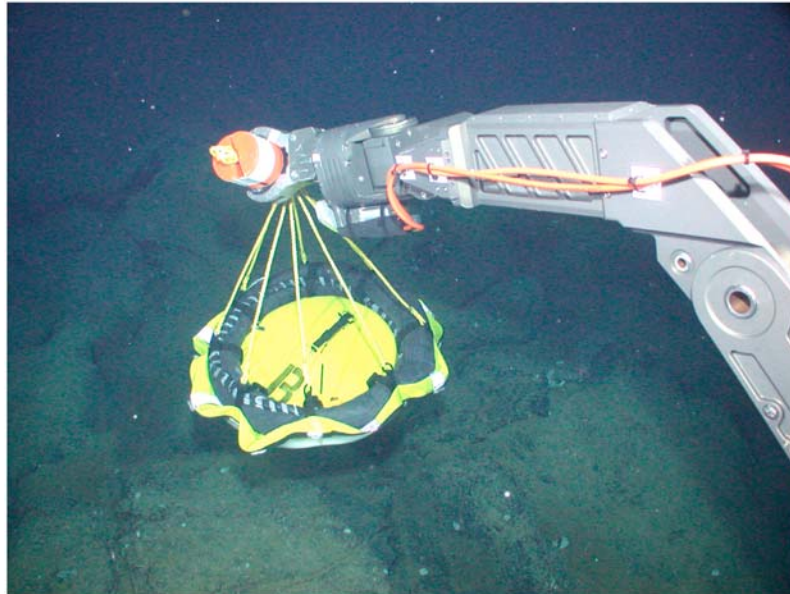
Figure 2. ROV *Jason II* manipulator, deploying thermal blanket on the Endeavour Segment of the Juan de Fuca Ridge. Black rod on top of blanket is Antares thermistor/logger.

[7] Measured heat flow values (Table 1) from the Endeavour axial valley and walls range from +16,000 mW/m² to zero mW/m², and include some stations with negative values. Negative heat flow values result when warm diffuse vent fluid wafts episodically past the upper thermistors of the blankets during the deployment period, and an example of this phenomenon is shown in Figure 4. Data from individual thermistors indicates that the below-blanket rock temperatures are quite cold for all sites with negative heat flow, and these sites have been classified, along with those of low conductive heat flow, as areas of possible recharge.

[8] The pervasive effects of fluid circulation within the spreading axis do not allow an a priori prediction of normal conductive heat flow values, which can be used for comparison with our local measurements. Theoretical values of total heat flux (both advective and conductive) suggest that the magmatic reservoir at a medium-spreading rate ridge axis should provide a total heat transport in excess of 5000 mW/m² [*Rabinowicz et al.*, 1999; *Morgan and Chen*, 1993]. However, heat flow values extrapolated inward from off-axis sedimented valleys to the axial valley suggest that 50 to 500 mW/m² is a more plausible range for
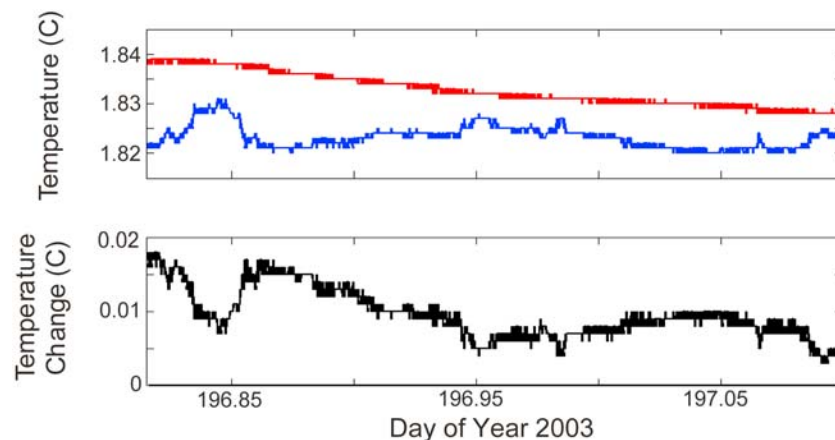

Figure 3. Example of conductive heat flow, station B6 (95 mW/m²). (top) Temperature versus deployment time. Red curve is temperature of thermistor below blanket, and blue is temperature on top of blanket. (bottom) Black curve is the difference between the two thermistors versus time.

Table 1. Heat Flow Data and Station Locations for All Thermal Blanket Sites[a]

Deployments	Latitude (m)	Longitude (m)	Depth (m)	ΔT (°C)	SD (°C)	Heat Flow (W/m²)
01-A1	492603	5310453	2192	0.169	0.078	1.7898
01-A2	492754	5310501	2210	0.004	0.001	0.0424
01-A3	492712	5310466	2213	0.005	0.003	0.053
01-A4	492870	5310861	2213	0.009	0.002	0.0953
02-A1	492754	5310341	2215	0.026	0.001	0.2754
02-A2	492643	5310444	2197	1.534	0.422	16.2448
02-A3	492687	5310447	2212	0.025	0.008	0.2621
02-A4	492862	5310455	2217	0.021	0.002	0.2171
02-A5	492939	5310450	2223	0.025	0.001	0.2648
02-A6	492470	5310466	2135	0.02	0.004	0.2118
02-A7	493159	5310490	2114	0.02	0.007	0.2065
03-B1	492408	5311016	2084	0.0137	0.0075	0.1451
03-A1	492477	5311013	2112	0.047	0.004	0.502
03-C1	492699	5310996	2174	0.621	0.01	6.5767
03-C2	492802	5311000	2198	0.009	0.003	0.0953
03-B2	492996	5310997	2212	0.011	0.001	0.1165
03-A2	493115	5310994	2212	0.005	0.001	0.0572
03-A3	493229	5311003	2146	−0.004	0.002	−0.0381
03-B3	493315	5311005	2129	−0.006	0.004	−0.0635
03-C3	493531	5310992	2106	−0.016	0.004	−0.1694
03-C4	493001	5310797	2229	0.019	0.002	0.2012
03-A4	492689	5310796	2196	−0.001	0.001	−0.0064
03-A5	493905	5311002	2215	0.065	0.015	0.6884
03-B5	492625	5310990	2171	0.0185	0.0149	0.1959
03-D5	492875	5310774	2211	0.011	0.002	0.1165
03-D6	493119	5310479	2125	−0.001	0.007	−0.0106
03-B6	492909	5310473	2207	0.009	0.002	0.0953
03-A6	492797	5310508	2208	−0.003	0.001	−0.0318
03-A7	492611	5310587	2192	0.1476	0.02	1.5632
03-C7	492797	5310607	2209	0.066	0.008	0.699
03-D7	492913	5310599	2219	−0.017	0.003	−0.1822
03-D8	492897	5310698	2218	0.001	0.003	0.0106
03-C8	492798	5310695	2214	0.023	0.004	0.2436
03-B8	492684	5310702	2198	0.094	0.018	0.9955
03-A8	492595	5310688	2180	−0.004	0.009	−0.0424
03-D9	492504	5310599	2127	−0.005	0.012	−0.053
03-C9	492697	5310501	2209	0.014	0.002	0.1483
03-B9	492688	5310502	2209	0.023	0.001	0.2436
03-A9	492669	5310499	2204	0.017	0.002	0.18
03-A10	492704	5310385	2212	0.009	0.001	0.0953
03-C10	492820	5310387	2207	0	0.001	0
03-B10	492755	5310380	2214	0.011	0.001	0.1165
03-D10	492587	5310376	2198	0.512	0.009	5.4224

[a]Latitude and longitude are in UTM meters for UTM zone 9. SD is one standard deviation of the data from the best fit polynomial in the heat flow versus 1/(time) plot. ΔT is the difference in equilibrium temperature between upper and lower thermistors.

conductive-only heat flow for sites distant from active advection [*Johnson et al.*, 1993], but this extrapolation should be viewed with caution. A histogram of the measured conductive heat flow values from this thermal blanket experiment suggests groupings into three categories, which are admittedly subjective: (1) sites less than +50 mW/m² including negative values are considered located on seafloor near zones of fluid recharge, (2) values between +50 mW/m² to 500 mW/m² are considered to be conduction-only sites, and (3) values more than 500 mW/m² are assumed to reflect active dis-

charge and are typically located at or near fluid discharge sites (Figure 5). Although the values of 500 and 50 mW/m² are somewhat arbitrary, a comparison to measured heat flow measurements taken outside the axial valley indicates that they are plausible limits to identify sources of fluid advection and recharge [*Johnson et al.*, 1993].

[9] The median for all measured heat flow values distributed over the axial valley is ~150 mW/m² while the mean is ~888 mW/m², although the latter value is dominated by a few high-value sites located
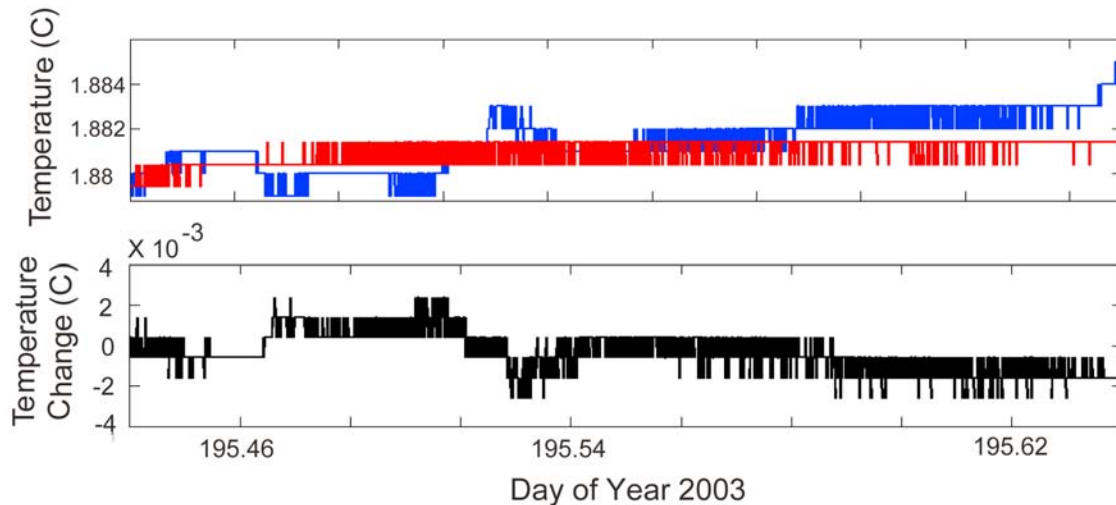
Figure 4. (top) Temperatures versus time of top (blue) and bottom (red) thermistors and (bottom) ΔT (black) for station A4, where extrapolated heat flow is near zero, interpreted as indicative of a fluid recharge zone. Note temperature scales and that discrete steps are due to the resolution of the A/D converter in the thermistor. Temperatures in Figure 4 (bottom) are shown $\times 10^{-3}$ for clarity.

near the vent fields. Taking the median value of ~150 mW/m² suggests that only ~3% of the total 5000 mW/m² heat flux through the axial valley is by conduction, with greater than ~97% of the heat of crustal formation at the axis transported by fluid advection. Although this extreme degree of partitioning has been recognized qualitatively for over 3 decades [*Lister*, 1974], this is the first semiquantitative measurement of the advection/conduction ratio in an unsedimented spreading center.

4. Measurement Practice and Errors

[10] In order to reach thermal equilibrium after placement on the seafloor, a thermal blanket deployment period of 6 h in length is considered a minimum at each site, although some deployment periods were considerably longer. The thermistor resolution of ±0.001°C limits the ability of the blankets to resolve absolute heat flow values less than ±10 mW/m². A variety of prototypes of the blanket were deployed on the Juan de Fuca and Gorda Ridges, and the deployment and data processing strategy are described in further detail elsewhere [*Johnson and Hutnak*, 1997, 1998; *Johnson et al.*, 2006; *Lowell et al.*, 2007]. Although the thermal blanket design is simple in concept, several potential sources of error can occur during field deployments. (1) At high heat flow sites, convection can occur within the open pores of the foam within the blanket; (2) a poor seal can occur between the

seafloor and the bottom of the blanket allowing heat to escape; and (3) minor warm fluid upwelling in very small rock fractures can occur unobserved beneath the blanket, adding to the heat transfer that is interpreted to be solely by conduction, suggesting that our estimates may include some low-temperature advection. In the field, near-bottom seawater temperature variations are the largest potential source of error and subjectively limit our confidence in interpreting the heat flow accuracy of this method to a conservative 10% to 20%.

[11] At the initial stages of development, we standardized on the urethane foam used (85 pores/inch;
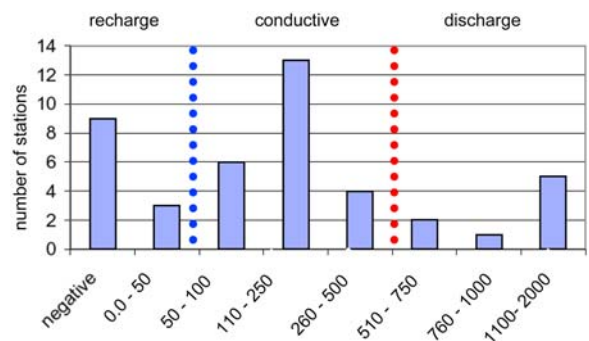

Figure 5. Histogram of Endeavour heat flow values. The *x* axis is in units of mW/m². Vertical blue line shows division between values interpreted as recharge (<+50 mW/m²) and conductive only (50–500 mW/m²). Red dotted line divides discharge areas (>500 mW/m²) from conductive-only values.

33.5 pores/cm), and calibrated the water-saturated thermal conductivity using a large (1800 L) tank overlying an aluminum plate that was uniformly heated from below at a known rate. At heat flow values < 10,000 mW/m^2, the conductivity of the saturated urethane foam was identical to that of water, and so we use the published value of seawater at 0°C (563 mW/m/°K) in our calculations. At heat flow values > 10,000 mW/m^2, we use an iterative process to determine the conductivity [*Johnson and Hutnak*, 1997, 1998]. The thermal blankets therefore have a useful dynamic measurement range of approximately three orders of magnitude; 10 mW/m^2 to 10,000 mW/m^2.

[12] When the thermal blankets are brought to the seafloor during the initial ROV descent through the water column, some residual heat from the surface is retained by the CaCl$_2$-saturated sealing ring. This results in an initial anomalous elevated temperature for the thermistors beneath the blanket, which decays toward thermal equilibrium with time. These initial elevated temperatures are similar to the sediment insertion heating that occurs with traditional heat flow probes, and the same processing techniques were used, i.e., curve fitting to the temperature versus time variation and extrapolation to infinite time as 1/time = zero. Similarly, when the thermal blankets are deployed in an area of very high heat flow (>1000 mW/m^2) and then subsequently moved to a lower heat flow site, some residual heat in the sealing ring can be retained, and thermal equilibrium is also determined by extrapolation. At two sites where the bottom thermistor temperatures continued to rise by several degrees over the entire 6 h deployment period, advection of warm hydrothermal fluid from nonvisible cracks in the seafloor beneath the blanket was assumed to have occurred, and those sites were not considered further in this manuscript.

[13] Our identification of sites of seawater recharge cannot distinguish between seawater inflow that feeds either the high-temperature fields or the low-temperature diffuse vents that surround them. The upper crust in the axial region of Endeavour Ridge is suggested by gravity measurements to be both porous (>10%) and likely permeable [*Holmes and Johnson*, 1993; *Johnson et al.*, 2000; *Pruis and Johnson*, 2002; *Gilbert and Johnson*, 1999], which would reduce any influence of along-axis faults to produce strong anisotropy in subsurface fluid flow. Although the present conductive heat flow measurements are the most extensive seafloor survey

conducted to date on bare rock seafloor, our necessarily two-dimensional results do not constrain the circulation pathways in the critical third dimension of depth. Our conductive heat flow data can be combined with recent seismic observations of a strongly sloping upper surface of the underlying magma chamber and near-seafloor magnetic field anomalies, and can provide additional constraints on patterns of subsurface fluid circulation. However, the present data only allow us to speculate on the depth of circulation and estimate fluid circulation residence times, parameters which are difficult to constrain without tracer type of experiments.

5. Results of the North Line Linear Array

[14] The results from the thermal blanket sites for the North Line station array located 300 m north of the N-MEF vent site are shown in Figure 6. Two stations on the western end of North Line were on the western boundary wall, and the three stations on the eastern end of the line were on the eastern wall of the axial valley. The easternmost station of this line lies outside the axial ridge and showed high heat flow indicative of crustal fluid circulation that is continuing in this unsedimented ridge flank site (Figure 6a), as has been noted in previous studies [*Villinger et al.*, 2002; *Johnson et al.*, 1993]. Three stations on the eastern axial valley wall had low heat flow values consistent with seawater recharge, and the three stations located on the valley floor showed systematically increasing heat flow to the west. Two stations located on the western wall indicated high conductive heat flow values (7,000 and 500 mW/m^2) associated with proximity to a fluid discharge zone, although no active fluid vents were observed by the ROV during deployment and recovery of the blankets. A zone of reduced magnetization, similar to those over the MEF vent fields, does mark this area however, suggesting past hydrothermal activity in the vicinity of the west rift valley wall [*Tivey and Johnson*, 2002]. A conductive-only station was measured on the summit of the western boundary ridge of the axial valley at the western end of the North Line (Figure 6b).

[15] These heat flow data from the North Line represent a single linear measurement profile imposed on what is certainly a complex three-dimensional process. However, the systematic variation in the linear array of measurements suggests a model where seawater is generally entrained into the porous upper crust within the eastern valley boundary faults,
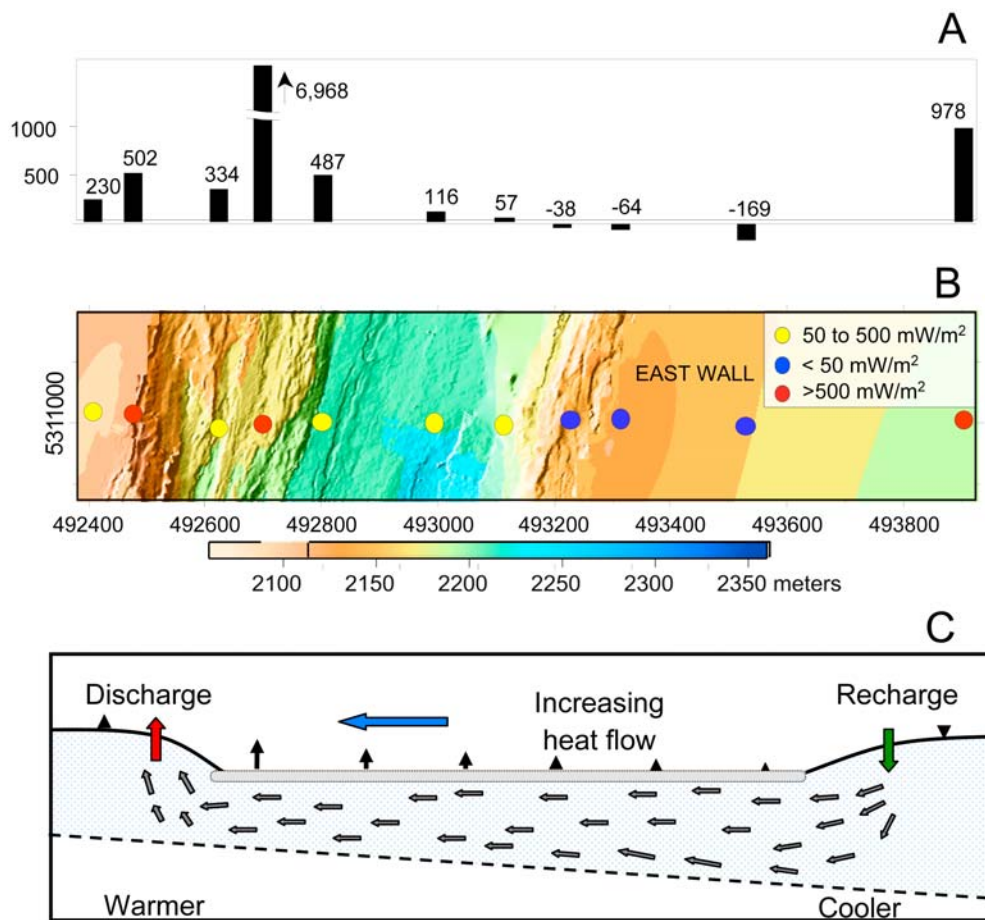
Figure 6. (a) Heat flow data from North Line. Units are mW/m² and are coordinated with the thermal blanket station positions in Figure 6b. The easternmost station lies in the topographic low east of the axial valley. (b) Station locations on a narrow swath of SM2000 bathymetry data. Colored circles correspond to recharge (blue), conductive (yellow), and discharge (red). (c) Interpretive cartoon of North Line data, with recharge occurring on the valley eastern boundary fault and lateral subsurface transport beneath the valley to discharge on the valley western boundary fault. Sloping dashed line represents the shallower magma chamber beneath the western side of the axial valley. Cartoon dimensions not to scale.

transported westward beneath largely unfractured surface lava flows of the valley floor and discharged as high-temperature fluid vents on the western boundary faults. The proposed east-west subsurface across-valley flow between the bounding rift valley faults suggested by our North Line heat flow data could be driven by the sloping (~30°) upper boundary of subsurface magma chamber, with higher-temperature vertical gradients on the western side of the axial valley [*Van Ark et al.*, 2007].

[16] The North Line thermal blanket transect displays an across axis variation in heat flow (Figure 6) that provides insight into what may be a fundamental pattern of subsurface hydrothermal fluid circulation across the entire Endeavour Ridge

axial valley. We suggest that the heat flow measurements reflect horizontal, cross-valley fluid transport within the shallow subseafloor driven by temperature gradients caused by the sloping top to the axial magma chamber as reported by *Van Ark et al.* [2007]. Seismic data show that the magma chamber reflector is 400 m shallower on the western edge of the axial valley compared to the eastern edge, which combined with a thinner seismic Layer 2A can establish an across-axis thermal gradient that can drive subsurface fluid flow [*Van Ark et al.*, 2007]. *Rabinowicz et al.* [1999] model this geometry and demonstrate analytically that a sloping thermal boundary layer at depth has the ability to drive fluid circulation across a rift valley.
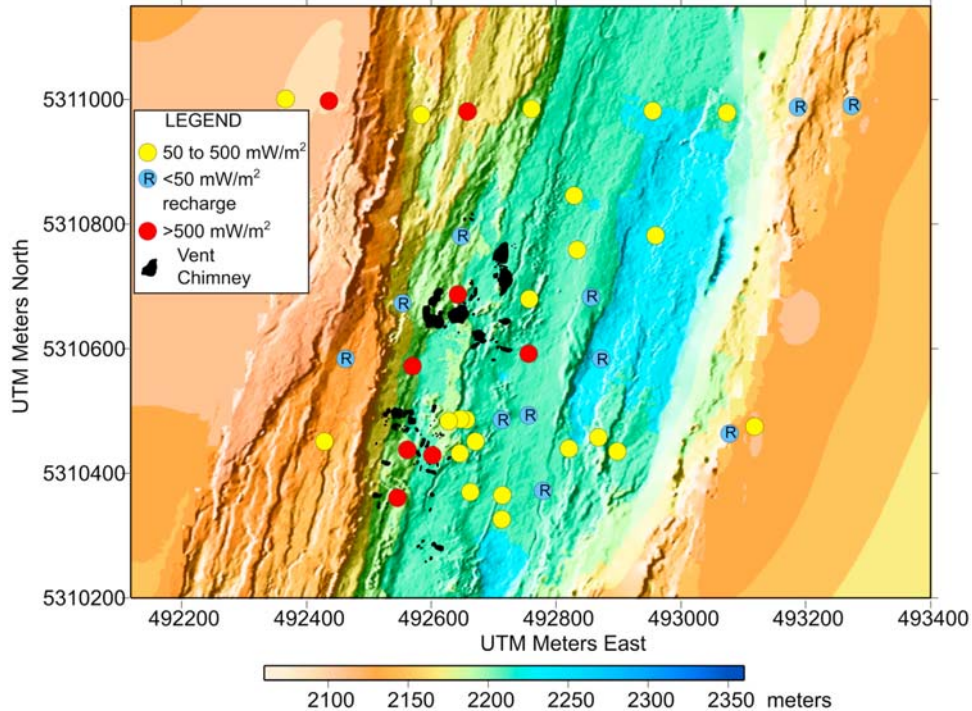
Figure 7. Thermal blanket stations around N-MEF, S-MEF, and NF plotted on a shaded SM2000 and Seabeam composite bathymetry map (color change every 20 m). Colors of heat flow data circles are as in Figure 6 with a circled R to designate recharge sites. Black areas are large sulfide structures. Recharge sites are distributed around N-MEF, adjacent to the central valley fissure, and near the eastern boundary faults.

[17] Thus, higher subcrustal temperatures on the western side of the axial valley can plausibly drive a generalized east-west horizontal fluid flow across the valley floor, from recharge on the eastern boundary faults to discharge on the western boundary faults (Figure 6c), producing the observed systematic east-west increase in the conductive heat flow of the North Line transect. This subsurface horizontal flow may be present over large areas of the axial valley where the subsurface magma chamber shows a high degree of east-west asymmetry in depth [*Van Ark et al.*, 2007]. Also, this cross-valley flow circulation would efficiently mine substantial amounts of heat from the underlying magma chamber. If this across-axis circulation model is correct, then the observation that all the high-temperature hydrothermal fields are presently located on the western side of the rift valley, including N-MEF and S-MEF, may represent localized hot spots superimposed on an overall east to west asymmetry in heat flow.

6. Results of the Main Endeavour Field Survey

[18] A completely systematic grid of measurements, with a nominal 100 m spacing around the MEF vent field (Figures 1 and 7) was not possible due to the need to avoid (1) sites of obvious fluid discharge and lateral near-bottom seawater entrainment; (2) sites where blankets could not obtain a seal to the seafloor including faults, fissures, and talus slopes; and (3) logistic limitations imposed by other cruise experiments. The highest heat flow values (several thousand mW/m^2) were obtained just outside aprons of sulfide debris from the high-temperature vents, both active and inactive, with the highest conductive heat value (~16,000 mW/m^2) located in S-MEF (Figure 7). Abundant fluid seeps and sulfide structures limited potential deployment sites directly adjacent to the N-MEF and S-MEF, but even within the hydrothermal fields, conductive heat flow values were not uniformly high. At N-MEF, where seafloor topography and the distribution of fluid discharge sites allowed some near-field thermal blanket deployments, conductive heat flow values were largely bimodal, with seafloor sites being

either very warm or very cold. Our thermal conductivity data did not show any direct impact of the magmatic and tectonic event that occurred within the Endeavour Segment in 1999 [*Johnson et al.*, 2000; *Lilley et al.*, 2003], although any thermal influence of that event would appear to be limited to a small portion of S-MEF [*Larson et al.*, 2009].

[19] N-MEF provides an example of a recharge zone distributed in a roughly annular distribution around an active high-temperature vent field. Recharge sites are located near the western boundary fault previously proposed as recharge for the MEF via slot convection [*Rabinowicz et al.*, 1999; *Wilcock*, 1998]. However, our conductive heat flow data shows sites of additional fluid recharge also form a roughly circular distribution around N-MEF, potentially supporting the annular convection model of *Coumou et al.* [2008]. Several sites associated with the large central valley fissure distant from the east/west bounding faults are also stations of very low heat flow (Figures 1 and 7). This central fissure runs parallel to the axis east of the MEF for a length of over 500 m, and ROV video observations show sections of the fissure that are open to widths of 1 to 2 m, suggesting that it is likely a conduit for seawater recharge into the subsurface fluid reservoir.

[20] It is important to note that not all recharge zones must supply high-temperature vents, and some seawater inflow may be supplying the low-temperature (<60°C) diffuse vents distributed around some large vent fields. Fluids that issue from low-temperature vents may not have penetrated deeply into the crust and the low conductive heat flow measurements associated with their recharge would be indistinguishable from the inflow that supports deeper, high-temperature vents. North of N-MEF, the NF vent site has a high conductive heat station (~6,000 mW/m^2) within a few tens of meters of a fluid discharge vent (260°C), and is flanked by two relatively low heat flow sites only 100 m distant (Figures 1 and 7). Sites located on the faulted eastern boundary wall of the MEF area also show low heat flow/recharge, similar to those on the east valley wall of the North Line sites. Considered in a simple 2-D interpretation, these very low heat flow sites on the valley boundary wall directly east of the MEF also support the suggestion of a pervasive east-west two-dimensional cross-valley flow, with seawater recharge on the eastern valley wall and fluid discharge near the western wall of the axial valley, similar to the pattern of the North Line data (Figure 6c).

7. Fluid Residence Times

[21] The spatial distribution of fluid recharge and discharge zones allow us to estimate fluid residence time in the subsurface (e.g., *Tolstoy et al.* [2008] for the East Pacific Rise). Residence time for fluid within the crustal reservoir is critical for studies of hydrothermal systems, but these calculations at best produce approximate average values. Actual transit times for individual fluid parcels can be an order of magnitude faster or slower, depending on the tortuosity of the individual pathways. Total heat output from the entire MEF system has been estimated at 590 MW [*Baker*, 2007], and we use an estimate of 300 MW (~50%) as a subset of that output for N-MEF. The radius of a concentric cylinder around the N-MEF defined by the thermal blanket recharge sites is ~300 m (Figure 7), and the temperature difference between seawater and high-temperature fluid is estimated at 350°C. No definitive crustal depth for hydrothermal fluid circulation at MEF has been obtained, but prior estimates include (1) the <500 m depth to Seismic Layer 2A/2B (extrusive/dike) boundary [*Van Ark et al.*, 2007; *Tivey and Johnson*, 2002], (2) the 1000 m upper limit of active crustal cracking [*Tolstoy et al.*, 2008; *Fisher et al.*, 2003; *Hutnak et al.*, 2006], or (3) the ~2000 m depth to a very thin conductive layer that overlies the axial magma chamber [*Tolstoy et al.*, 2008; *Wilcock et al.*, 2009].

[22] The N-MEF, S-MEF and NF discharge areas appear to be located within their own individual crustal alteration zones based on magnetic data that indicate discrete zones of reduced magnetization in these areas [*Tivey and Johnson*, 2002]. This suggests that cylindrical high-temperature fluid upwelling zones are probably isolated from each other at least in the uppermost crust. Studies of off-axis crustal fluid flow argue that the highest permeability, porosity and hydrothermal fluid flow occur largely in the uppermost part of the extrusive seismic Layer 2A [*Fisher et al.*, 2003; *Hutnak et al.*, 2006]. Seismic velocity studies on the Endeavour axis and flanks indicate that the lowest seismic velocities and highest crustal porosities are also in the upper 500 m of the extrusive crust [*Van Ark et al.*, 2007] implying that most, but not all, of the volume of the relevant hydrothermal fluid reservoir may lie above the seismic Layer 2A boundary and the hydrothermal system may have a narrow root below this upper crustal zone (Figure 8).

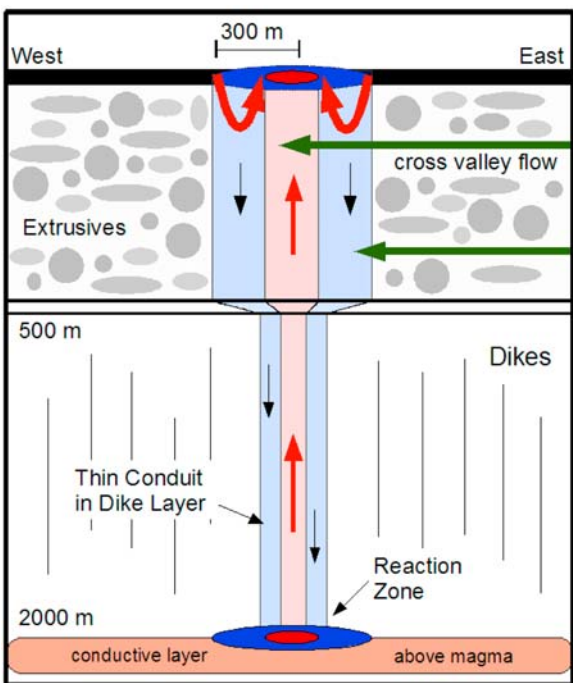[23] Similar arguments, based on data from Ocean Bottom Seismometer (OBS) arrays at the East

Figure 8. Cartoon of "nested" model of the subcrustal hydrothermal fluid circulation at MEF. Uppermost thick dark line represents the seafloor. Green horizontal arrows represent cross-valley flow, which can supply either the deeply sourced upwelling high-temperature fluid or the recharge fluid for the same system. Grey blobs represent porous extrusive basalts, and thin vertical lines represent the sheeted dike section. Bright red arrows near the seafloor are the shallow circulation cells that feed the diffuse low-temperature venting adjacent to the large vent fields.

Pacific Rise (EPR) spreading center and with theoretical models, can be made for hydrothermal fluid that circulates within a crustal reservoir shaped as a tall cylinder, extending uniformly vertical from the surface vents to just above the underlying magma chamber [*Tolstoy et al.*, 2008; *Coumou et al.*, 2008]. Since there is no direct evidence for the shape or depth of the subsurface crustal reservoir, we will use the short cylinder with a deep but narrow root in calculating fluid residence times (Figure 8). An even larger uncertainty in any residence time calculation is the estimate of porosity of the crust involved in the fluid circulation, with seafloor gravity data supporting a 10% or higher value [*Holmes and Johnson*, 1993; *Cochran et al.*, 1999; *Gilbert and Johnson*, 1999], while many previous studies have used a value of 1% porosity [*Wilcock*, 1998; *Wilcock et al.*, 2009; *Tolstoy et al.*, 2008; *Hutnak et al.*, 2006].

$$t_r = \frac{V \rho c \Delta T}{H} \qquad (1)$$

Residence time t_r is calculated using equation (1), where ρ (675 kg/m^3) and c (6400 J/(kg °K)) are the fluid density and heat capacity of the fluid, ΔT is the mean temperature difference between the seafloor and reaction zone (350°C), V is the volume of the reservoir, and H is the observed heat flow [*Tolstoy et al.*, 2008]. This simple approximation ignores the strong temperature dependence of viscosity and density, since temperature distribution within the reservoir is largely unknown.

[24] Although poorly constrained, the importance of residence time for hydrothermal fluids to chemical, biological and geothermal studies argues that we attempt to estimate the range of possible values. For a shallow cylindrical reservoir extending only 460 m deep to the Layer 2A/2B boundary beneath the N-MEF with a narrow root [*Van Ark et al.*, 2007], we calculate a residence time of 2.1 years for 10% crustal porosity, and 76 days for 1% porosity (Figure 8). Residence times for the across-axis flow suggested by the North Line data (Figure 6) are unbounded as there are no lateral constraints to the size of the flow channel and no vent fluid temperatures available. Recently, *Foustoukos et al.* [2009] used CO_2/CO equilibrium data to obtain residence times for the very shallow circulation cells that feed low-temperature (~50°C) diffuse vents adjacent to the large Endeavour high-temperature fields, and estimated that they could be as short as a few tens of hours. These residence times are orders of magnitude shorter than our estimates, and support the previous arguments based on chemistry that the low-temperature diffuse vents are supported by a different subsurface circulation system than the large higher-temperature vents [*Kelley et al.*, 2002].

8. Conclusions

[25] Our bare rock conductive heat flow survey of the Juan de Fuca Ridge spreading axis covers an area of 1 km by 1 km that encompasses several large fields of hydrothermal fluid discharge within a fault-bounded axial valley. In contrast to the localized fluid discharge sites, thermal blanket stations showing low conductive heat flow, interpreted as seawater recharge zones, are distributed throughout the axial valley in a systematic pattern. These recharge zones are located (1) on the western boundary fault, (2) surrounding the large MEF sys-

tems, (3) adjacent to the central valley fissure, and (4) on the eastern boundary fault. Taken as individual subsets, the conductive heat flow measurements can be interpreted as supporting nested modes of hydrothermal cellular circulation ranging from (1) pervasive across-axis flow beneath the valley floor, (2) annular concentric ring circulation around high-temperature vent fields, and (3) shallow penetration related to diffuse vents found adjacent to high-temperature fields. Our conductive heat flow data does not directly discriminate between these different models, but suggests a more comprehensive model that includes most of these modes may be appropriate.

[26] In conclusion, our new bare rock heat flow data also strongly suggests a subsurface hydrothermal circulation pathway that is generally oriented across the rift valley and flows within the upper crustal rocks from east to west. We suggest this geometry is fundamentally driven by the depth to the axial magma chamber, which appears to be systematically shallower beneath the western edge of the rift valley and 400 m deeper beneath the eastern edge of the valley. We further suggest that the MEF and other high-temperature fields on the western boundary fault are localized "hot spot" punctuations within this generalized across-axis flow. We also conclude that conductive heat flow is a minor contribution to the Endeavour axis heat budget, providing less than 3% of the total heat flux, with the remaining ~97% due to fluid advection. However, while the total amount of energy transfer due by conductive heat flow is small, the spatial distribution of seawater recharge zones that these measurements provide are a significant boundary condition to subsurface hydrothermal fluid flow during oceanic crustal formation.

Acknowledgments

References

Baker, E. T. (2007), Hydrothermal cooling of mid-ocean ridge axes: Do measured and modeled heat fluxes agree?, *Earth Planet. Sci. Lett.*, *263*, 140–150, doi:10.1016/j.epsl. 2007.09.010.

Cochran, J. R., D. J. Fornari, B. J. Coakley, R. Herr, and M. A. Tivey (1999), Continuous near-bottom gravity measurements made with a BGM-3 gravimeter in DSV *Alvin* on the East Pacific Rise crest near 9°31′N and 9°50′N, *J. Geophys. Res.*, *104*(B5), 10,841–10,861, doi:10.1029/1999JB900049.

Coumou, D., T. Driesner, and C. A. Heinrich (2008), The structure and dynamics of mid-ocean ridge hydrothermal systems, *Science*, *321*, 1825–1828, doi:10.1126/science. 1159582.

Fisher, A. T., et al. (2003), Hydrothermal recharge and discharge across 50 km guided by seamounts on a young ridge flank, *Nature*, *421*, 618–621, doi:10.1038/nature01352.

Foustoukos, D. I., N. J. Pester, K. Ding, and W. E. Seyfried Jr. (2009), Dissolved carbon species in associated diffuse and focused flow hydrothermal vents at the Main Endeavour Field, Juan de Fuca Ridge: Phase equilibria and kinetic constraints, *Geochem. Geophys. Geosyst.*, *10*, Q10003, doi:10.1029/2009GC002472.

Gilbert, L. A., and H. P. Johnson (1999), Direct measurements of oceanic crustal density at the northern Juan de Fuca Ridge, *Geophys. Res. Lett.*, *26*(24), 3633–3636, doi:10.1029/1999GL008391.

Holmes, M. L., and H. P. Johnson (1993), Upper crustal densities derived from sea floor gravity measurements: Northern Juan de Fuca Ridge, *Geophys. Res. Lett.*, *20*, 1871–1874, doi:10.1029/93GL00909.

Hutnak, M., A. T. Fisher, L. Zuhlsdorff, V. Spiess, P. H. Stauffer, and C. W. Gable (2006), Hydrothermal recharge and discharge guided by basement outcrops on 0.7–3.6 Ma seafloor east of the Juan de Fuca Ridge: Observations and numerical models, *Geochem. Geophys. Geosyst.*, *7*, Q07O02, doi:10.1029/2006GC001242.

Johnson, H. P., and M. Hutnak (1997), Conductive heat loss in recent eruptions at mid-ocean ridges, *Geophys. Res. Lett.*, *24*, 3089–3092, doi:10.1029/97GL02998.

Johnson, H. P., and M. Hutnak (1998), Measuring conductive heat flow, *Sea Technol.*, *39*, 23–28.

Johnson, H. P., K. Becker, and R. P. Von Herzen (1993), Near-axis heat flow measurements on the northern Juan de Fuca Ridge: Implications for fluid circulation in oceanic crust, *Geophys. Res. Lett.*, *20*(17), 1875–1878, doi:10.1029/93GL00734.

Johnson, H. P., M. Hutnak, R. P. Dziak, C. G. Fox, I. Uruyo, J. P. Cowen, J. Nabelek, and C. Fisher (2000), Earthquake-induced changes in a hydrothermal system at the Endeavour Segment, Juan de Fuca Ridge, *Nature*, *407*, 174–177, doi:10.1038/35025040.

Johnson, H. P., J. A. Baross, and T. A. Bjorklund (2006), On sampling the ocean crustal reservoir, *Geofluids*, *6*, 251–271.

Kelley, D. S., J. A. Baross, and J. R. Delaney (2002), Volcanoes, fluids, and life at mid-ocean ridge spreading centers, *Annu. Rev. Earth Planet. Sci.*, *30*, 385–491, doi:10.1146/annurev. earth.30.091201.141331.

Larson, B. I., M. D. Lilley, and E. J. Olson (2009), Parameters of subsurface brines and hydrothermal processes 12–15 months after the 1999 magmatic event at the Main Endeavour Field as inferred from in situ time series measurements of chloride and temperature, *J. Geophys. Res.*, *114*, B01207, doi:10.1029/2008JB005627.

Lilley, M. D., D. A. Butterfield, J. E. Lupton, and E. J. Olson (2003), Magmatic events can produce rapid changes in hydro-

thermal vent chemistry, *Nature*, *422*, 878–881, doi:10.1038/nature01569.

Lister, C. R. B. (1974), On the penetration of water into hot rock, *Geophys. J. R. Astron. Soc.*, *39*, 465–509.

Lowell, R. P., P. A. Rona, and R. P. Von Herzen (1995), Seafloor hydrothermal systems, *J. Geophys. Res.*, *100*, 327–352, doi:10.1029/94JB02222.

Lowell, R. P., S. Gosnell, and Y. Yang (2007), Numerical simulations of single-pass hydrothermal convection at mid-ocean ridges: Effects of the extrusive layer and temperature-dependent permeability, *Geochem. Geophys. Geosyst.*, *8*, Q10011, doi:10.1029/2007GC001653.

Morgan, J. P., and Y. L. Chen (1993), The genesis of oceanic crust: Magma injection, hydrothermal circulation, and crustal flow, *J. Geophys. Res.*, *98*, 6283–6297, doi:10.1029/92JB02650.

Pruis, M. J., and H. P. Johnson (2002), Age dependent porosity of young upper oceanic crust: Insights from seafloor gravity studies of recent volcanic eruptions, *Geophys. Res. Lett.*, *29*(5), 1076, doi:10.1029/2001GL013977.

Rabinowicz, M., J.-C. Sempere, and P. Genthon (1999), Thermal convection in a vertical permeable slot: Implications for hydrothermal circulation along mid-ocean ridges, *J. Geophys. Res.*, *104*(B12), 29,275–29,292, doi:10.1029/1999JB900259.

Tivey, M. A., and H. P. Johnson (2002), Crustal magnetization reveals sub-surface structure of the Juan de Fuca hydrothermal fields, *Geology*, *30*, 979–982, doi:10.1130/0091-7613(2002)030<0979:CMRSSO>2.0.CO;2.

Tolstoy, M., F. Waldhauser, D. R. Bohnenstiehl, R. T. Weekly, and W.-Y. Kim (2008), Seismic identification of along-axis hydrothermal flow on the East Pacific Rise, *Nature*, *451*, 181–184, doi:10.1038/nature06424.

Van Ark, E. M., R. S. Detrick, J. P. Canales, S. M. Carbotte, A. J. Harding, G. M. Kent, M. R. Nedimovic, W. S. D. Wilcock, J. B. Diebold, and J. M. Babcock (2007), Seismic structure of the Endeavour Segment, Juan de Fuca Ridge: Correlations with seismicity and hydrothermal activity, *J. Geophys. Res.*, *112*, B02401, doi:10.1029/2005JB004210.

Villinger, H., I. Grevemeyer, N. Kaul, J. Hauschild, and M. Pfender (2002), Hydrothermal heat flux through aged oceanic crust: Where does the heat escape?, *Earth Planet. Sci. Lett.*, *202*(1), 159–170, doi:10.1016/S0012-821X(02)00759-8.

Wilcock, W. S. D. (1998), Cellular convection models of mid-ocean ridge hydrothermal circulation and temperatures of black smoker fluids, *J. Geophys. Res.*, *103*, 2585–2596, doi:10.1029/97JB03252.

Wilcock, W. S. D., E. E. E. Hooft, D. R. Toomey, P. R. McGill, A. H. Barclay, D. S. Stakes, and T. M. Ramirez (2009), The role of magma injection in localizing black-smoker activity, *Nat. Geosci.*, *2*, 509–513, doi:10.1038/ngeo550.

Williams, D. L., K. Green, T. H. van Andel, R. P. Von Herzen, J. R. Dymond, and K. Crane (1979), The hydrothermal mounds of the Galapagos Rift: Observations with DSRV *Alvin* and detailed heat flow studies, *J. Geophys. Res.*, *84*, 7467–7484.